arXiv:1806.10694v1 [physics.ins-det] 27 Jun 2018

Imaging individual Ba atoms in solid xenon for barium tagging in nEXO

C. Chambers,[1] T. Walton,[1,*] D. Fairbank,[1] A. Craycraft,[1] D. Harris,[1] J. Todd,[1] A. Iverson,[1] W. Fairbank,[1] J.B. Albert,[2] G. Anton,[3] I.J. Arnquist,[4] I. Badhrees,[5] P. Barbeau,[6] D. Beck,[7] V. Belov,[8] T. Bhatta,[9] F. Bourque,[10] J. P. Brodsky,[11] E. Brown,[12] T. Brunner,[13,14] A. Burenkov,[8] G.F. Cao,[15] L. Cao,[16] W.R. Cen,[15] S.A. Charlebois,[10] M. Chiu,[17] B. Cleveland,[18,†] M. Coon,[7] M. Côté,[10] W. Cree,[5] J. Dalmasson,[19] T. Daniels,[20] L. Darroch,[13] S.J. Daugherty,[2] J. Daughhetee,[9] S. Delaquis,[21,‡] A. Der Mesrobian-Kabakian,[18] R. DeVoe,[19] J. Dilling,[14] Y.Y. Ding,[15] M.J. Dolinski,[22] A. Dragone,[21] J. Echevers,[7] L. Fabris,[23] J. Farine,[18] S. Feyzbakhsh,[24] R. Fontaine,[10] D. Fudenberg,[19] G. Gallina,[14] G. Giacomini,[17] R. Gornea,[5,14] G. Gratta,[19] E.V. Hansen,[22] M. Heffner,[11] E. W. Hoppe,[4] J. Hößl,[3] A. House,[11] P. Hufschmidt,[3] M. Hughes,[25] Y. Ito,[13,§] A. Jamil,[26] M.J. Jewell,[19] X.S. Jiang,[15] S. Johnston,[24,¶] A. Karelin,[8] L.J. Kaufman,[2,21] D. Kodroff,[24] T. Koffas,[5] S. Kravitz,[19,**] R. Krücken,[14] A. Kuchenkov,[8] K.S. Kumar,[27] Y. Lan,[14] A. Larson,[9] D.S. Leonard,[28] G. Li,[19] S. Li,[7] Z. Li,[26] C. Licciardi,[18] Y.H. Lin,[22] R. MacLellan,[9] T. Michel,[3] B. Mong,[21] D. Moore,[26] K. Murray,[13] R.J. Newby,[23] Z. Ning,[15] O. Njoya,[27] F. Nolet,[10] O. Nusair,[25] K. Odgers,[12] A. Odian,[21] M. Oriunno,[21] J.L. Orrell,[4] G. S. Ortega,[4] I. Ostrovskiy,[25] C.T. Overman,[4] S. Parent,[10] A. Piepke,[25] A. Pocar,[24] J.-F. Pratte,[10] V. Radeka,[17] E. Raguzin,[17] T. Rao,[17] S. Rescia,[17] F. Retière,[14] A. Robinson,[18] T. Rossignol,[10] P.C. Rowson,[21] N. Roy,[10] R. Saldanha,[4] S. Sangiorgio,[11] J. Schneider,[3] A. Schubert,[19,††] D. Sinclair,[5] K. Skarpaas,[21] A.K. Soma,[25] G. St-Hilaire,[10] V. Stekhanov,[8] T. Stiegler,[11] X.L. Sun,[15] M. Tarka,[24] T. Tolba,[15] T.I. Totev,[13] R. Tsang,[4] T. Tsang,[17] F. Vachon,[10] V. Veeraraghavan,[25] G. Visser,[2] J.-L. Vuilleumier,[29] M. Wagenpfeil,[3] Q. Wang,[16] J. Watkins,[5] M. Weber,[19] W. Wei,[15] L.J. Wen,[15] U. Wichoski,[18] G. Wrede,[3] S.X. Wu,[19] W.H. Wu,[15] X. Wu,[15] Q. Xia,[26] L. Yang,[7] Y.-R. Yen,[22] O. Zeldovich,[8] X. Zhang,[15,‡‡] J. Zhao,[15] Y. Zhou,[16] and T. Ziegler[3]

(nEXO Collaboration)

[1] *Physics Department, Colorado State University, Fort Collins, Colorado 80523, USA*
[2] *Department of Physics and CEEM, Indiana University, Bloomington, IN 47405, USA*
[3] *Erlangen Centre for Astroparticle Physics (ECAP), Friedrich-Alexander University Erlangen-Nürnberg, Erlangen 91058, Germany*
[4] *Pacific Northwest National Laboratory, Richland, WA 99352, USA*
[5] *Department of Physics, Carleton University, Ottawa, Ontario K1S 5B6, Canada*
[6] *Department of Physics, Duke University, and Triangle Universities Nuclear Laboratory (TUNL), Durham, North Carolina 27708, USA*
[7] *Physics Department, University of Illinois, Urbana-Champaign, Illinois 61801, USA*
[8] *Institute for Theoretical and Experimental Physics named by A. I. Alikhanov of National Research Center Kurchatov Institute, Moscow 117218, Russia*
[9] *Department of Physics, University of South Dakota, Vermillion, South Dakota 57069, USA*
[10] *Université de Sherbrooke, Sherbrooke, Québec J1K 2R1, Canada*
[11] *Lawrence Livermore National Laboratory, Livermore, CA 94550, USA*
[12] *Department of Physics, Applied Physics and Astronomy, Rensselaer Polytechnic Institute, Troy, NY 12180, USA*
[13] *Physics Department, McGill University, Montréal, Québec H3A 2T8, Canada*
[14] *TRIUMF, Vancouver, British Columbia V6T 2A3, Canada*
[15] *Institute of High Energy Physics, Beijing, China*
[16] *Institute of Microelectronics, Beijing, China*
[17] *Brookhaven National Laboratory, Upton, New York 11973, USA*
[18] *Department of Physics, Laurentian University, Sudbury, Ontario P3E 2C6, Canada*
[19] *Physics Department, Stanford University, Stanford, California 94305, USA*
[20] *Department of Physics and Physical Oceanography, UNC Wilmington, Wilmington, NC 28403, USA*
[21] *SLAC National Accelerator Laboratory, Menlo Park, California 94025, USA*
[22] *Department of Physics, Drexel University, Philadelphia, Pennsylvania 19104, USA*
[23] *Oak Ridge National Laboratory, Oak Ridge, TN 37831, USA*
[24] *Amherst Center for Fundamental Interactions and Physics Department, University of Massachusetts, Amherst, MA 01003, USA*
[25] *Department of Physics and Astronomy, University of Alabama, Tuscaloosa, AL 35487, USA*
[26] *Department of Physics, Yale University, New Haven, CT 06511, USA*

[27] Department of Physics and Astronomy, Stony Brook University, SUNY, Stony Brook, New York 11794, USA
[28] IBS Center for Underground Physics, Daejeon 34047, Korea
[29] LHEP, Albert Einstein Center, University of Bern, Bern, Switzerland
(Dated: June 25, 2019)

The identification, or "tagging", of the ^{136}Ba daughter atom that results from double beta decay of ^{136}Xe provides a promising technique for the elimination of backgrounds in a future upgrade of the nEXO neutrinoless double beta decay experiment. The tagging scheme being developed in this work utilizes a cryogenic probe to trap the barium atom in solid xenon and extract it from the time projection chamber filled with liquid xenon. The barium atom is then tagged via fluorescence imaging in the solid xenon matrix. Individual barium atoms in a particular matrix site have been imaged and counted with high definition by scanning a focused laser across the solid xenon matrix deposited on a sapphire window. This is the first time single atoms have been imaged in solid noble element and represents significant progress towards a practical barium tagging technique for nEXO.

The search for neutrinoless double beta decay ($0\nu\beta\beta$) is an important probe into the nature of neutrinos. Observation would imply that neutrinos are Majorana particles, would demonstrate violation of lepton number conservation, and could help determine the absolute neutrino mass [1]. EXO-200 is searching for $0\nu\beta\beta$ in ^{136}Xe with 110 kg of active liquid Xe (LXe) enriched to 80.6% ^{136}Xe in a time projection chamber (TPC). Two-neutrino double beta decay ($2\nu\beta\beta$) of ^{136}Xe has been observed in EXO-200, and its half-life is measured at $T_{1/2}^{2\nu\beta\beta} = 2.165 \pm 0.016(\text{stat}) \pm 0.059(\text{sys}) \times 10^{21}$ yr [2]. The most recent EXO-200 $0\nu\beta\beta$ search sets a limit on the half-life at $T_{1/2}^{0\nu\beta\beta} > 1.8 \times 10^{25}$ yr (90% CL), which corresponds to an effective Majorana neutrino mass of $\langle m_{\nu_e} \rangle < 147\text{-}398$ meV, depending on nuclear matrix element calculations [3].

A ^{136}Xe TPC provides a unique opportunity to tag the daughter ^{136}Ba at the site of a double beta decay event. The implementation of this Ba tagging would improve $0\nu\beta\beta$ sensitivity by effectively eliminating all backgrounds except $2\nu\beta\beta$ [4]. Ba tagging is being investigated for a future upgrade of the next-generation LXe experiment, nEXO, a 5 tonne enriched Xe experiment recently described in [5, 6]. Initial results have been reported for research on methods of Ba tagging in LXe [7, 8], and also in a Xe gas TPC [9]. The NEXT collaboration has recently reported images of single Ba^{++} in fluorescent dye molecules from a dilute deposit of barium perchlorate salt solution [10].

This paper presents a major step towards realization of Ba tagging in solid Xe (SXe) for nEXO [7]. In this method, a cryogenic probe would be moved to the position of the $0\nu\beta\beta$ candidate event in LXe, and the daughter atom or ion would be captured in a small amount of SXe on a sapphire window at the end of the probe [11, 12]. It would then be detected by its laser-induced fluorescence in the SXe. It is expected that a Ba^{++} ion will convert to Ba^{+} in LXe, as the LXe conduction band gap is less than the ionization potential for Ba^{+} [4]. Neutralization to Ba may also occur in the charge cloud following a $\beta\beta$ event. A study of ^{214}Bi daughters of ^{214}Pb β-decay in EXO-200 has reported that 76(6)% of these daughters are ionized, with negligible subsequent neutralization after many minutes [13]. Thus, a large fraction of ^{136}Ba $0\nu\beta\beta$ daughters is expected to be in the singly ionized state in LXe. Whether or not the ^{136}Ba will remain ionized in SXe on a cold probe is not yet known.

Significant progress on understanding the spectroscopy of Ba in SXe has been made [7, 14, 15]. Through theoretical modeling, the strongest fluorescence peaks at 577 and 591 nm are identified as Ba atoms in 5-atom and 4-atom vacancy sites in the SXe matrix [15]. These two fluorescence peaks bleach fairly rapidly at high laser intensity, e.g. using a focused laser beam [7]. Obtaining large numbers of photons from single Ba atoms in these matrix sites would benefit from a method to overcome bleaching, e.g., with repumping lasers. In contrast, the peak at 619 nm experiences less bleaching. In this work, imaging of single Ba atoms in SXe via the 619 nm fluorescence peak is reported. This is the first time that single atoms have been imaged in a solid noble element matrix. Images of single dye molecules in solid argon have been obtained previously [16].

* now at Prism Computational Sciences Madison, WI
† also at SNOLAB, Ontario, Canada
‡ Deceased
§ now at JAEA
¶ now at Argonne National Lab
** gnow at Lawrence Berkeley National Lab
†† now at OneBridge Solutions, Boise, ID
‡‡ now at Tsinghua University, Beijing, China

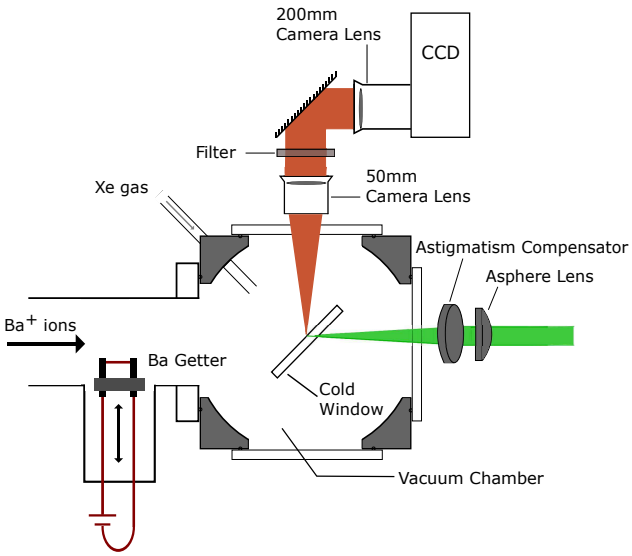

FIG. 1: Experimental setup for depositing Ba/Ba^+ in SXe matrices and for excitation and imaging of the deposited atoms/ions.

I. APPARATUS AND METHOD

The apparatus for depositing and observing Ba/Ba^+ deposits in SXe is described in [7]. Important components are shown in Fig. 1. The source of Ba is an ion beam at 2 keV energy, filtered to select Ba^+ with an E×B velocity filter. A set of pulsing plates produces ∼1 µs ion bunches for depositing small numbers of ions. The spectra of Ba^+ ion deposits in the SXe matrix exhibit peaks known to be due to neutral Ba atoms [7]. Thus some percentage of the ions neutralize in the matrix, although the fraction has not yet been determined. An alternative source of neutral Ba is a $BaAl_4$ getter wire which can be moved into the beam path and heated to emit Ba atoms toward the sample. However, it is challenging to achieve low Ba flux with this source and to calibrate it.

Deposits are made on a cold sapphire window tilted at 45° with respect to the Ba^+ beam. To create a sample, Xe gas is directed toward the window by opening a leak valve. The Xe gas freezes onto the window and forms a SXe matrix with a thickness of around a micron. This is initiated a few seconds prior to the Ba deposit, continues during the Ba deposit, and is turned off a few seconds after the Ba deposit by closing the valve.

In this work, deposition is done with the sapphire window at a temperature of ∼50 K. This reduces hydrogen, nitrogen and oxygen content in the matrix, as these residual gases condense below 50 K in vacuum [7]. The window is then cooled to 11 K for observation. Xe is deposited at a rate of around 60 nm/s. An experiment cycle consists of a deposit at 50 K, a fluorescence observation at 11 K, and then evaporation of the deposit by heating the window to 100 K. Many deposits are made in a day with varying numbers of ions deposited, as well as periodic SXe-only deposits to establish the background.

The area density of deposited Ba^+ ions cannot be measured directly because the window is an insulator. During the deposit, only the induction signal of the pulse of ions in transit through a circular induction plate is recorded. To estimate the deposited ion density, the pulsed ion beam is sampled before and after deposits by two Faraday cups located 17.5 cm and 4.5 cm before the window. The factor for conversion of these signals to ion density on the window is measured in a separate calibration procedure in which the window is replaced by a third Faraday cup at the window position, and the alignment and magnitude of the three cup signals are compared under conditions similar to that of actual deposits. The uncertainty in the Faraday cup measurements is estimated as ±10% due to secondary electron effects, measured by biasing the Faraday cup electrodes. An additional +0 to −10% uncertainty in the ion density deposited on the observation window is included for possible misalignment of the ion beam relative to the excitation laser by 1 mm, with an average ion beam diameter of 5.1 mm at the window location.

The number of Ba^+ ions deposited within the 1/e radius of the laser beam gives a rough upper limit to the number of Ba atoms responsible for the observed signal with a fixed laser beam. For typical ion bunch densities of 0.1-1 fC/mm^2 and focused laser $1/e^2$ radii of $w_{0x} = 3.2$ µm and $w_{0y} = 3.8$ µm, this results in about 0.001-0.01 Ba^+ ions/pulse in the 1/e intensity laser region.

The excitation laser, a Coherent 599 cw dye laser with Rhodamine 6G dye, pumped by the 532 nm line of a Coherent Verdi-V8 laser, enters from the back side of the window. To position the laser beam with sub-µm precision, two computer controlled piezoelectric translation stages are used to move the laser focusing lens. Ba fluorescence light is collected and collimated by a 50 mm Nikon camera lens. A filter with a sharp-edged band-pass of 610-630 nm passes just the 619 nm fluorescence peak. A 200 mm Nikon camera lens then focuses the light onto a liquid nitrogen cooled CCD [17], resulting in an image of 4× magnification. Each of the 20×20 µm pixels of the CCD represents approximately a 5×5 µm area on the SXe sample.

For a given laser intensity, the smallest focus possible is desired for optimal signal-to-background ratio from single atoms. To achieve this, an aspherical lens of 7.9 cm focal length [18] is used to minimize spherical aberration, and a fused silica optical flat of 1 cm thickness is placed at 9° after the lens in order to compensate for astigmatism caused by the tilted sapphire window (Fig. 1).

Vibrations of the sapphire window relative to the excitation laser increase the area of laser exposure, and reduce the average intensity seen by a single Ba atom. The main source of vibration is the cryostat He compressor cycle, which pulses with a frequency of about 2.25 Hz. To limit the laser exposure to a segment of the cryostat cycle with minimal vibration, a shutter is placed in the laser path and synchronized with the signal from an accelerometer on the outside of the cryostat. This laser gating has 45% duty cycle.

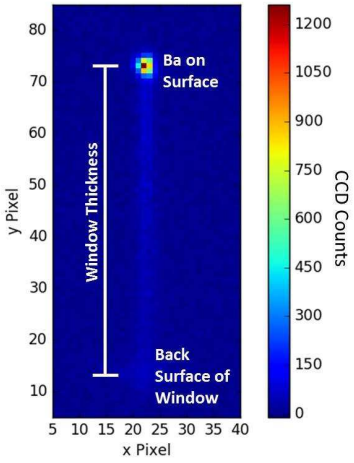

FIG. 2: Example CCD image of a Ba^+ deposit in SXe on a tilted c-plane sapphire window of 0.5 mm thickness, excited by a focused 570 nm laser, using a 620 nm fluorescence band-pass filter.

A. Backgrounds

A typical CCD image recorded with a focused laser beam at 570 nm is shown in Fig. 2. A strong signal from the barium deposit in SXe on the front surface of the window is visible, along with weak emission from the opposite window surface. Very low concentrations of Cr^{3+} in the sapphire bulk (sub-ppb level) produce a sharp fluorescence peak at 693 nm, with a broad tail extending to the 610-630 nm region passed by the band-pass filter. This results in the faintly visible line through the window in the CCD image. Commercially available c-plane quality sapphire from Meller Optics and Rubicon Technologies has been found to have sufficiently low Cr^{3+} concentrations for detecting single Ba atoms.

The background emission from the front sapphire surface beneath the SXe layer is the main challenge for single Ba imaging. It has been found that this background can be reduced significantly and semi-permanently by photo-bleaching. A variety of wavelengths have been used effectively for bleaching, including 514.5 nm, 532 nm, 570-572 nm, and 580.5 nm. A typical bleaching procedure consists of a repeating raster scan of an 80 mW 532 nm laser, focused to around $w_0 = 10$ µm, in a 14×14 position grid, with 8 µm grid spacing and 20 s at each position per scan. This is done with the sapphire window at 100 K. As seen in a subsequent imaging scan in Fig. 3, this reduces the surface background ∼30× over a region of about 90×90 µm. This area is large enough to accommodate both the fixed laser and scanned images presented in Sec. II.

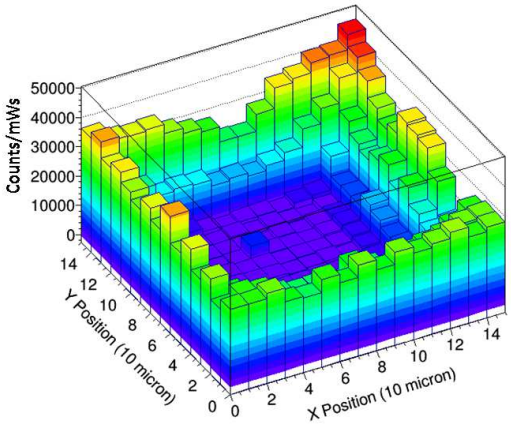

FIG. 3: Scan image of background emission after bleaching with 532 nm laser light. A ∼30× reduction of the background is observed in the low area where the bleaching laser was scanned.

II. RESULTS

A. Fixed Laser Images

The signal in Fig. 2 corresponds to a deposit of 152^{+15}_{-30} Ba^+ ions into the laser region, and is there-

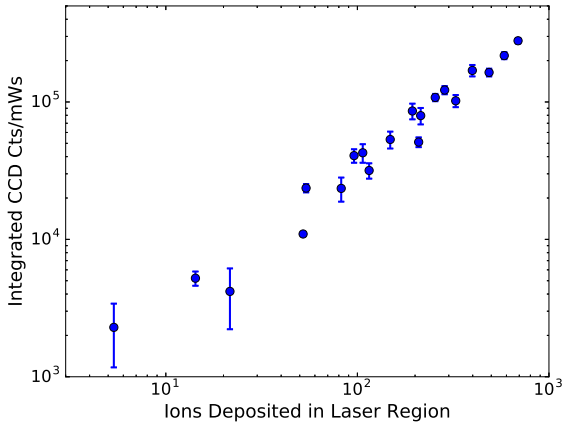

FIG. 4: 619 µm Ba fluorescence vs. number of Ba^+ ions deposited.

fore due to less than or equal to this number of Ba atoms. A Gaussian fit to the image gives a $1/e^2$ radius of 10.4 µm, which is larger than the average laser beam radius of w = 3.5 µm. Aberrations and vibrations in the collection optics and imperfections in the surface of the SXe layer could contribute to blurring of the image.

The Ba fluorescence in a given deposit is determined by summing the counts in a 4 × 4 pixel area enclosing the laser spot and subtracting the SXe-only background. The background is measured by averaging the summed CCD counts in the focused laser region from the prior and following SXe-only deposits for each Ba^+ deposit. A typical background level is ∼900 counts/mWs. The observed Ba counts per mWs of laser exposure vs. Ba^+ ions deposited in the laser region are plotted in Fig. 4. Each point represents a separate Ba^+ deposit with the signal averaged over 4 laser positions separated by 20 µm on the deposit. The error bar is the standard deviation of the four measurements. The observed signal is linear with a log-log slope of 1.04 ± 0.05. The slope of the linear fit is 379 ± 10 counts/mWs per ion. For these measurements, ∼40 µW of focused 572 nm laser excitation was used with ∼3 s of laser exposure.

For a practical Ba tagging application in nEXO, it is crucial for each Ba tag to be independent of any previous tagging measurements or residual barium on the cryogenic probe to ensure the Ba daughter is correlated to the decay candidate being investigated. The raw CCD images of a large deposit of ≤ 7000 Ba atoms, along with the background in SXe-only deposits made before and after the Ba deposit are

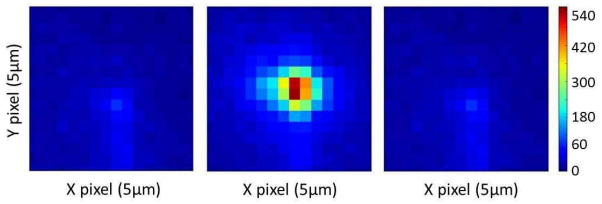

FIG. 5: CCD Image of a Ba^+ deposit yielding ≤ 7000 Ba atoms (center) with its preceding (left) and succeeding (right) SXe-only deposits. All three images have the same intensity scale shown at the right of the figure. Exposures are 1 s with around 1 µW of 570 nm laser excitation.

shown in Fig. 5. Significantly, the background level of the surrounding SXe-only deposits are similar, demonstrating that evaporation of the SXe matrix removes detectable Ba atoms from the sample window, even at densities much higher than anticipated in nEXO.

B. Scanned Images

By further decreasing the density of Ba ions deposited, single Ba atoms can be spatially resolved. To image these atoms, the laser is rastered across the deposit. A typical scan consists of a square grid of 12 × 12 steps with 3 s of laser exposure and a spacing of 4 µm. The raw CCD images of four successive steps of a laser scan are shown in Fig. 6. As the laser passes over the Ba atom, a strong 619 nm signal appears. When the laser moves off of the Ba atom, the observed counts return to background level.

A scan image of this region is generated by integrating the CCD counts in a 4×4 pixel area encompassing the laser region in each frame. These integrals are divided by the laser exposure, and arranged according to the position of each spot in the grid. Five such scan images, taken from a typical run, are shown in Fig. 7. Data from the four frames shown in Fig 6 contribute to four points in line y=7 in Fig. 7(b). In the first SXe-only deposit, no fluorescence peaks are found in the scan (Fig. 7(a)). After this, the deposit is evaporated by heating the sapphire window to 100 K. Then, a new SXe deposit with 12 Ba^+ pulses, corresponding to 48^{+5}_{-10} Ba^+ ions in the full scan area is produced. Two large peaks due to single Ba atoms are observed in a scan of this deposit (Fig. 7(b)). This scan is then repeated, and the Ba peaks persist, as seen in Fig. 7(c).

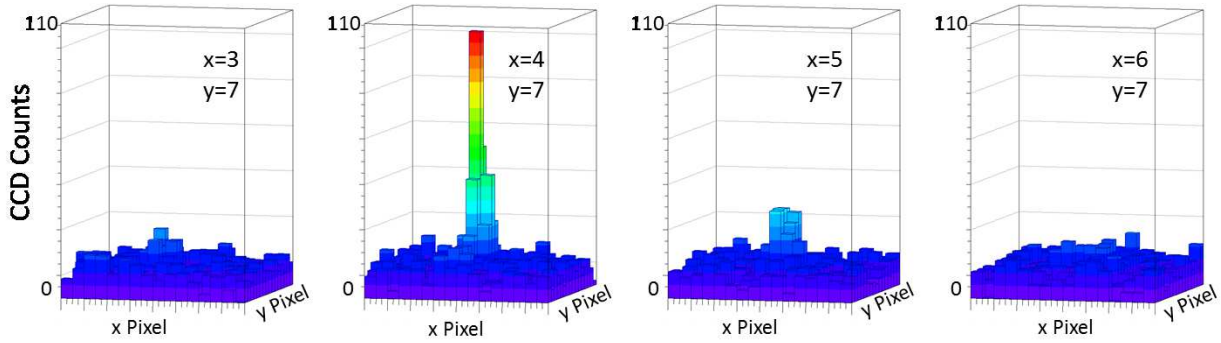

FIG. 6: Raw CCD images of successive steps of a raster scan of a Ba in solid Xe deposit, as the laser passes over a Ba atom from left to right. The (x,y) coordinates refer to the laser position in 4 µm scan steps.

At this point, the laser is moved to the location of the Ba peak on the left, and many 3 s exposures are taken. The time dependence of the integrated signal from a 3 × 3 pixel area of the single Ba peak is shown in Fig. 8. The signal level agrees with the single Ba peak value, and persists for ∼30 s, including the prior two scans, before abruptly dropping to the background level. This fast turn-off of the fluorescence signal is a hallmark of single atoms. About 3300 photons (0.5 CCD counts/photon) are detected from this atom. This corresponds to around 1.4×10^6 photons absorbed and emitted by one atom. For comparison, the standard deviation of the SXe-only background in Fig. 8 for a 30 s integration is 45 detected photons, and for the different laser positions in the SXe-only scans in Fig. 7 (a) and (e) is 30 detected photons in a 3 s integration.

Following this fixed laser position run, a third scan is done, and the Ba peak on the left has disappeared, as expected. The right Ba peak on the edge of the scan persists, as seen in Fig.7 (d). After evaporating this deposit, a new SXe-only deposit is made. As in the previous SXe-only deposit, no peaks are observed in this scan (Fig.7 (e)). This illustrates the lack of any "history effect" due to previous Ba deposits and the absence of any signal from possible Ba contamination on the sapphire window.

C. Time Resolved Photon Counting

The decay lifetimes of both the sapphire surface background and the average signal from many Ba atoms were investigated using a 561 nm pulsed laser with 100 ps pulse length as the excitation source, and a single photon avalanche photodiode (SPAD) as the detector. The time between the laser pulse and the arrival of a photon at the SPAD was measured by a fast counter, and a histogram of photon arrival times was recorded [19]. The decay histograms for a SXe-only (green) and Ba in SXe (blue) deposit, are shown in Fig. 9. By subtracting the SXe-only histogram from the Ba histogram, the decay lifetime for the 619 nm emission of Ba was isolated and measured to be 7.0 ± 0.3 ns. The SXe-only background decay is comprised of more than one decay constant, but is nonetheless significantly shorter than the Ba decay lifetime. By time gating the CCD or SPAD, the signal to background ratio can be increased by a factor of 2 with a loss of 50% of the barium signal. In the future, a sapphire window will be mounted at the end of a cryoprobe [7], likely to be made of some type of metal. Background emission from the metal tubing may be a concern for Ba atom detection. The observed lifetime of emission at 619 nm from a stainless steel cryoprobe tube, shown in Fig. 9 (red), is ∼1.5 ns. Thus, background from the stainless steel parts of a cryoprobe could be reduced by time gating with minimal Ba signal loss.

III. DISCUSSION

The Ba sample in this work is deposited as Ba^+ ions. The fluorescence lines of Ba^+ in SXe are expected in the blue-green region rather than the yellow-red region. Thus a spectroscopic assignment of the 619 nm emission line to Ba rather then Ba^+ is favored. To further test this, a spectrum of a neutral Ba deposit made with the Ba getter source is compared in Fig. 10 to a spectrum of a Ba^+ deposit. Identical spectra are observed using the two

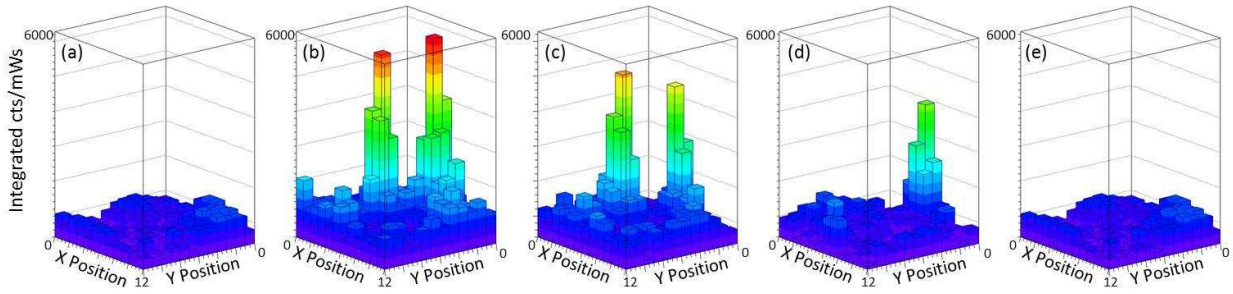

FIG. 7: Scan images of a sequence of laser scans. The step size is 4 µm, with a 12×12 grid. First, a scan of a SXe-only deposit is done (a) and evaporated. Another deposit is done with Ba in SXe and scanned twice, (b) and (c). A third scan of the Ba in SXe deposit was then done (d) after observing the left Ba atom peak for 150 s, during which observation it disappeared. The Ba in SXe sample was then evaporated and another SXe-only deposit made and scanned (e).

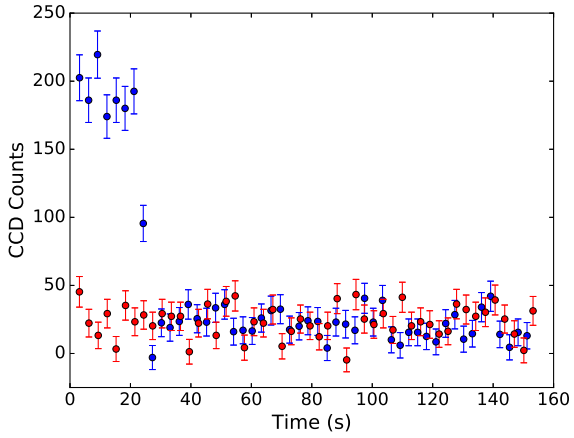

FIG. 8: Fluorescence signal from a single Ba peak (blue) and a SXe-only deposit (red). In these runs, the laser exposure per frame is 5.5×10^{-2} mW s

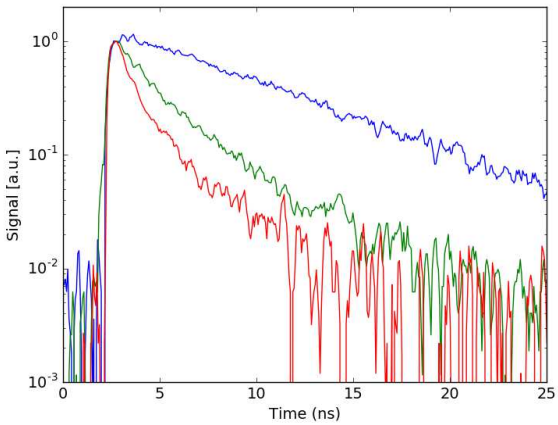

FIG. 9: Histograms of 619 nm fluorescence decays of Ba in SXe (blue), SXe-only (green), and cryoprobe tube (red).

sources under similar conditions. This confirms the 619 nm emission line as associated with Ba atoms resulting from neutralization of the incident Ba^+ ions. In addition, no fluorescence peak is observed from deposits of Ar^+ ions in SXe at 2000 eV under similar conditions. This rules out matrix damage as the source of the 619 nm peak. Thus, a reasonable assignment of the 619 nm emission line is to Ba atoms in a different matrix site to those already identified theoretically. In the following paragraphs, alternate Ba molecule interpretations are considered, and found to be inconsistent with observations.

Assignment to Ba_2 is unlikely as a linear relationship of signal vs. ions deposited is observed in Fig. 4, rather than quadratic. At the low ion density of Fig. 7, implanted Ba^+ ions are separated, on average, by 8 µm. Since the Ba^+ ions are implanted 7 ± 5 nm [20] below the surface of the SXe, mobility of the neutralized Ba atoms should be limited.

Reactions of deposited Ba with residual gas impurities, such as water and oxygen to form molecules should also be considered. A limit of < 100 ppm residual gas molecules in the SXe matrix is established through fringe rate and pressure comparisons. The most likely species to form are BaOH and BaO, through the reactions

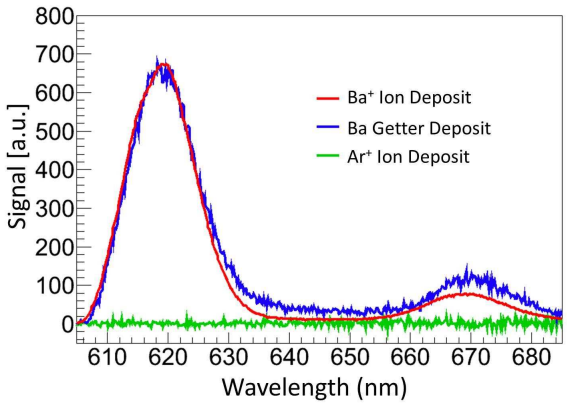

FIG. 10: Spectra of deposits from three different sources in SXe. The Ba getter deposit spectrum is scaled since the deposited Ba density cannot be determined.

$$\begin{aligned} \mathrm{Ba} + \mathrm{H_2O} &\rightarrow \mathrm{BaOH} + \mathrm{H} \\ \mathrm{Ba} + \mathrm{O_2} &\rightarrow \mathrm{BaO} + \mathrm{O} \end{aligned} \quad (1)$$

Both processes are endothermic [21], and thus energetically unfavored. BaOH vapor has known emission bands in the green at 487 nm and 512 nm, and in the IR at 712-758 nm and 783-839 nm [22]. These do not agree with the observed 619 nm emission. At low temperature, the upper state of BaO should be primarily the $A^1\Sigma^+(\nu')$ state. This state has a multi-line spectrum in vacuum with calculated values from 455 - 865 nm [23]. The ν'=0 to ν''=2 and 4 transitions are close to our observed peaks at 619 nm and 670 nm, but adjacent transitions are missing. Furthermore, the excitation spectra of these peaks are different, contradicting a common ν'=0 upper state for the emission. The $A^1\Sigma^+$ state lifetime of 356 ns in vacuum [24], is discrepant with the 7 ns decay lifetime of the observed 619 nm emission line presented in this work. Thus, this line is not due to BaO.

IV. CONCLUSIONS

The 619 nm emission peak observed in deposits of Ba^+ and Ba in SXe is attributed to neutral Ba atoms in a stable SXe matrix site. The imaging and counting of individual atoms with high definition in a particular matrix site by scanning a focused laser has been demonstrated. This is the first imaging of individual atoms in solid rare gas. Successful detection of individual Ba atoms in SXe at this level is a significant step toward Ba tagging in nEXO.

ACKNOWLEDGEMENTS

This material is based upon work supported by the National Science Foundation under Grant Number PHY-1132428 and the U.S. Department of Energy, Office of Science, Office of High Energy Physics under Award Number DE-FG02-03ER41255. The authors are grateful to Picoquant for the loan of the time resolved photon counting equipment.

[1] K. Nakamura *et al.* (Particle Data Group), *Chin. Phys. C* **40**, 100001 (2016) (http://pdg.lbl.gov).
[2] J. Albert *et al.* (EXO-200 Collaboration), *Phys. Rev. C* **89**, 015502 (2014).
[3] J. Albert *et al.* (EXO-200 Collaboration), *Phys.Rev.Lett.* **120**, 072701 (2018).
[4] M. Moe, *Phys. Rev. C* **44**, R931 (1991).
[5] S. Al Kharusi *et al.* (nEXO Collaboration), arXiv:1805.11142 *[physics.ins-det]* (2018)
[6] J. Albert *et al.* (nEXO Collaboration), *Phys. Rev. C* **97**, 065503 (2018)
[7] B. Mong *et al.*, *Phys. Rev. A* **91**, 022505 (2015).
[8] K. Twelker *et al.*, *Review of Scientific Instruments* **85**, 095114 (2014).
[9] T. Brunner *et al.*, *International Journal of Mass Spectrometry* **379**, 110-120 (2015).
[10] A.D. MacDonald *et al.* (NEXT Collaboration), *Phys.Rev.Lett.* (2018).
[11] K. Wamba, (PhD Dissertation), Stanford University, (2006).
[12] P.C. Rowson, Stanford Linear Accelerator Center, *Cryogenic Ion Capture Probe R&D at SLAC*, SLAC-PUB-17110, (2017).
[13] J. Albert *et al.* (EXO-200 Collaboration), *Phys. Rev. C* **92**, 045504 (2015).
[14] B.Davis, J. McCaffery, *J. Chem. Phys.* **144**, 1044308 (2016); doi: 10.1063/1.4940688
[15] B. Davis,B. Gervais, J. McCaffrey, *J. Chem. Phys.* **148**, 124308 (2018); doi: 10.1063/1.5019890
[16] J. Sepiol *et. al.*, *Chem. Phys. Lett.* **311**, (1999); doi: 10.1016/S0009-2614(99)00753-8
[17] Roper Scientific SPEC-10 LN-Cooled Spectroscopy Detector

[18] Thorlabs part ASL10142-A.
[19] Picoquant PicoHarp 300, PDL800D laser and PDM detector.
[20] J.F. Ziegler, M.D. Ziegler, J.P. Biersack, SRIM- the stopping and range of ions in matter. *Nucl. Instr. Meth. Phys. Res. B*, **268**, (2010)
[21] E. Murad, *J. Chem. Phys.* **75**, 4080 (1981); doi: 10.1063/1.442567
[22] Monique Charton and A.G. Gaydon, *Proc.Phys. Soc. A* **69**, 520 (1956)
[23] Katsumi Sakurai, S.E. Johnson, and H.P. Broida, *J. Chem. Phys.* **52**, 1625 (1970); doi: 10.1063/1.1673196
[24] S.E. Johnson, *J. Chem. Phys.* **56**, 149 (1972); doi: 10.1063/1.1676841